Materials Research. 2024; 27:e20240088
DOI: https://doi.org/10.1590/1980-5373-MR-2024-0088

Study of Work-Hardening Rate Transient of AISI 409 Stainless Steel Under Strain Path Changes

***Frederick Louis Dias de Morais*[a], *Elaine Carballo Siqueira Corrêa*[a], *Wellington Lopes*[a*]**

[a]*Centro Federal de Educação Tecnológica de Minas Gerais, Av. Amazonas, 5253, 30421-169, Belo Horizonte, MG, Brasil*

Received: February 22, 2024; Revised: May 24, 2024; Accepted: May 27, 2024

Metal forming processes present many changes in the strain path necessary to obtain the dimensions and shape of a metal part. The loading mode, the amount of prestrain, the initial state of a material and its respective substructural arrangements affect the mechanical properties of different products. Many phenomena, such as the Bauschinger Effect, occur during a metal forming operation when the materials are subject to a mix of mechanical efforts. These events can be associated with changes in the dislocation substructure and crystallographic orientations. Considering the effect of strain path changes on the responses of metallic parts, this work investigates the mechanical behaviour of AISI 409 steel submitted to a loading route composed of cold rolling, tensile and shearing operations, modifying the direction of the last loading. The results indicated the effect of tensile effort and the respective dislocation substructure on the occurrence of work-hardening rate transient for the shearing carried out at 0° and a minor effect for the shearing conducted at 45° due to non-significant changes on the dislocation substructure.

Keywords: *Strain path, work-hardening, AISI 409.*

1. Introduction

Strain path changes are commonly detected in stamping operations and are necessary to obtain the shape and dimensions of workpieces. However, strain paths can promote heterogeneities in the distribution of plastic deformation and the occurrence of transients in the work-hardening rate[1,2]. The substructural arrangement and crystallographic texture assumed by materials during a metal-forming operation influence the formability of different steels and non-ferrous alloys. The knowledge of structural characteristics supports, for example, the selection of materials for specific products and the appropriate adjustment variables of the process[3,4].

Considering the transient flow behaviour, this phenomenon is a continued variation in work-hardening during plastic deformation processes, which is associated with dynamic recovery, strain path changes (deformation states, intensity, and prestrain mode, for example), the presence of non-metallic inclusions, and metallurgical characteristics[5,6].

The evolution of the work-hardening and substructural arrangement assumed by a material after successive strain paths allow the occurrence of phenomena such as the Bauschinger Effect and work-hardening transients[7,8]. The intensity of these phenomena can be measured through the impact of strain path changes using references such as the α parameter, indicated by the scalar product of the strain tensors before and after the strain path change, as shown in the Equation 1. In this situation, the parameter α is evaluated by the cosine of the angle between two vectors representing the initial and the final deformation modes, which varies from 1 (monotonic loading) to -1 (reversed: Bauschinger loading)[9].

$$\alpha = \frac{\varepsilon_p . \varepsilon}{\left|\varepsilon_p\right| . \left|\varepsilon\right|} \quad (1)$$

In equation (1), ε_p and ε are the strain tensors for pre-straining and final straining, respectively.

Achieving a full characterization of work-hardening from initial yielding up to the strength limit is essential for the effective design of metal forming products that experience a complex stress-strain loading. Considering this, the goal of this work was to investigate the mechanical behaviour and the occurrence of work-hardening transient of ferritic stainless steel, AISI 409 after successive strain path changes composed by cold rolling, tensile and shearing, modifying the direction of the last mechanical effort.

2. Materials and Methods

2.1. Material and structural analysis

As received (cold rolled) AISI 409 ferritic stainless steel sheets 1.0mm thick were used in this work. This material is typically used in gas exhaust systems in explosion engines and stamping in general. The chemical composition exhibited (% in weight): 0.014%C, 0.168%Mn, 0.465%Si, 11.00%Cr, 0.138%Ni and 0.163%Ti obtained through optical emission spectrometry (MIP OES).

*e-mail: wellingtonlopes@cefetmg.br

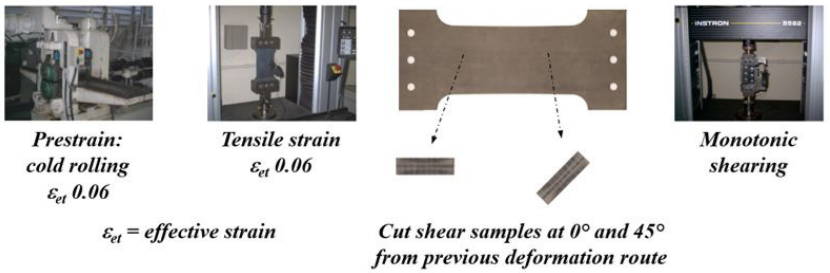

Figure 1. Flowchart for rolling/tensile/shear route.

Microstructural characterization used conventional metallographic preparation methods, the chemical attack carried out with Vilella (1g picric acid, 5mL concentrated hydrochloric acid and 100 mL PA ethyl alcohol) and procedures for measuring grain size according to ASTM E112[10]. The analysis and acquisition of images were performed in an optical (OM), a scanning electron microscope (SEM) and transmission electron microscopy (TEM) images were acquired on a FEI Tecnai G2 F20 microscope, using an accelerating voltage of 200 kV and typical magnification of 10kX to 40kX.

The phase detection of AISI 409 steel was performed in a diffractometer with Cu Kα radiation (λ = 1.5418Å) with the 2-theta range of 40° ~ 120° with steps of 0.02°, using the PCPDFWIN version 2.2 software from ICDD (International Council for Diffraction Data).

2.2. Loading route

The loading route used in this work is exhibited in Figure 1. It is composed of cold rolling, tensile, and shearing in two directions concerning the last mechanical effort: 0° and 45° from the rolling direction (RD). This mechanical route generated two α parameters: 0 (high severity, shearing conducted at 0°) and 0.5 (medium severity, shearing conducted at 45°).

2.3. Mechanical tests and cold rolling

Vickers microhardness tests were performed using a load of 100 gf, the penetration time was 15 s, involving 12 indentations in the annealed sample, spaced 0.2 mm each other.

Tensile tests were performed in an Instron 5982 universal testing machine with a Blue Hill 3 control system. An automatic Instron 2630-100 extensometer was used in the experiments to acquire deformation values. The initial deformation rate for all tensile tests was $10^{-3}s^{-1}$.

Two models of specimens for uniaxial tension were used in this work: model A (used for mechanical characterization in the initial state, ASTM E-8[11], and B (used to promote changes in the strain path). This specimen was employed to allow the removal of samples for the shear test at 0° and 45° concerning the direction of the previous deformation in tensile, Figure 2. All tensile specimens were made by submerged cutting by wire EDM using the Robofil 240 SL Charmilles machine.

The anisotropy tests were carried out with the specimen cut at 0° (RD), 45°, and 90° (transverse direction, TD).

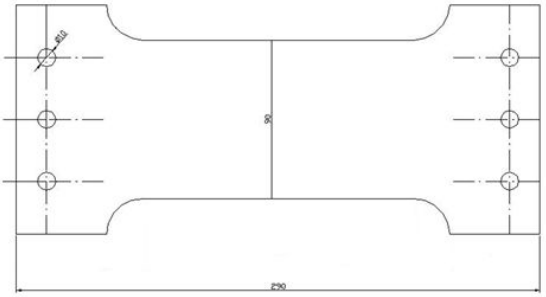

Figure 2. Schematic sample for tensile test, type B.

The Lankford values (r-value) were measured on the specimens deformed at a permanent engineering strain of 0.12. The weighted average or normal anisotropy (r_m) and the earing tendency or planar anisotropy (Δr) were further calculated according to ASTM E517-19[12].

The Hollomon strain-hardening exponent value (n value) and the work-hardening rate, $d\sigma/d\varepsilon$ or θ, were identified according to Zandrahimi et al.[13]. The term $d\sigma/d\varepsilon$. $1/\sigma$ (normalized work-hardening rate, i.e., work-hardening rate multiplied by the inverse of effective stress) when it is smaller than unity defines the work-hardening exponent, n value.

Additionally, the analysis of transient in the work-hardening rate was investigated using the instantaneous strain-hardening exponent, $n_{inst,}$ to express a continuous variation of n value during plastic deformation processes such as the metal forming operations that exhibit a mix of mechanical efforts analogous to those exposed in this work. This exponent is obtained from differentiation Hollomon, Equation 2[14,15].

$$n_{inst} = \frac{ln(\sigma_m - \sigma_{m-1})}{ln(\varepsilon_m - \varepsilon_{m-1})} \quad (2)$$

where σ_m is the true stress at a given point m and ε is the corresponding true strain.

The shearing tests required a particular fixture mounted on the Instron machine. This shear device was designed similarly to one developed by Bouvier et al.[16]. The shearing specimens were cut with a shearing machine and were 50mm long, 20mm wide and t, thickness, which value depends on the condition of the material (rolled and rolled/tensioned). For the rolling/tensile/shearing loading route, the samples

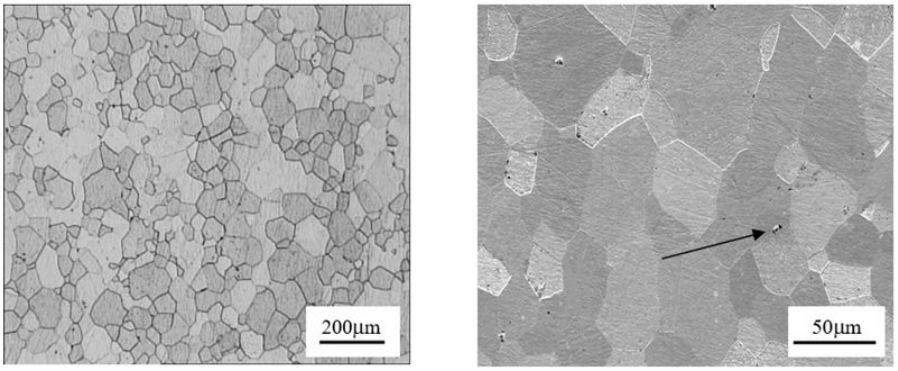

Figure 3. (a) optical microscopy and (b) scanning electron microscopy for AISI 409, revealing the presence of titanium nitride (TiN) as indicated by the arrow.

were extracted from the tensile sheet at 0°and 45° from the tensile direction.

Cold rolling was performed in a Frohling rolling mill with 200mm diameter cylinders and a rolling speed of 6.25m/min. This rolling step followed the same initial rolling direction, RD, of the material, 0° RD. The effective (true) von Mises rolling strain, e_r, was equal to 0.06, calculated according to Equation 3 (t_0: initial thickness and t_f: final thickness). This strain value was chosen to establish a dislocation density typical of this plastic deformation mode[17].

$$e_r = (2/\sqrt{3}).ln(t_0/t_f) \quad (3)$$

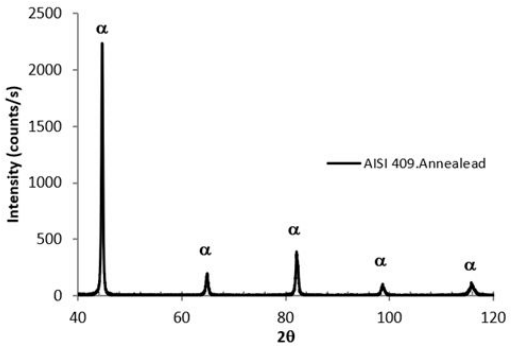

Figure 4. XRD diffractogram AISI 409.

3. Results and discussion

3.1. Characterization AISI 409 steel

Figure 3 shows the microstructural aspects of stainless steel 409 observed through optical and scanning electron microscopy in the as-received state. Analysis by an energy dispersive spectrometer detected the presence of titanium nitride, TiN, indicated by the arrow in Figure 3b. This result was correlated with the solidification of the alloy in the steelmaking environment.

The corresponding XRD result from the AISI 409 steel is shown in Figure 4. This material exhibited a ferritic microstructure (α) consisting of fine equiaxed grains with a medium size of 57 mm and Vickers hardness of 147HV–0.1 ± 1 HV. When submitted to strain path changes, the typical mechanical behaviour of metallic alloys depends on several variables such as the mode, prestrain value, and grain size. A large ferrite grain size, for example, affects the intensity of transients in the work hardening rate[18], which was not observed in this material.

The mechanical properties of AISI 409 steel measured at 0°, 45° and 90° regarding the rolling direction, RD, are presented in Table 1. The results for the anisotropy factor suggested a moderate thickness reduction as indicated by the r_m value and the tendency for the occurrence of "ears" at 0° and 90°RD in a deep drawing operation, as reported by $\Delta r > 0$, Table 2.

Table 1. Mechanical properties from annealed AISI 409 steel samples extracted from different angles concerning the rolling direction.

Rolling Direction	Yield strength, YS (MPa)	Work-hardening exponent, n
0° RD	220 ± 2	0.247
45° RD	245 ± 2	0.237
90° RD	225 ± 3	0.240

Table 2. Anisotropy parameters of AISI 409 steel.

$R_{0°}$	$R_{45°}$	$R_{90°}$	Δr	r_m
1.715	1.521	2.620	0.647	1.844

3.2. Effect of prestrain mode on the mechanical behaviour of AISI 409

The effect of the prestrain mode on the mechanical behaviour of AISI 409 steel was investigated using rolling/shear and tensile/shear loading routes at 0°RD. In Figure 5, it is possible to verify that the prestrain in both modes of deformation increased the mechanical strength of AISI 409 when

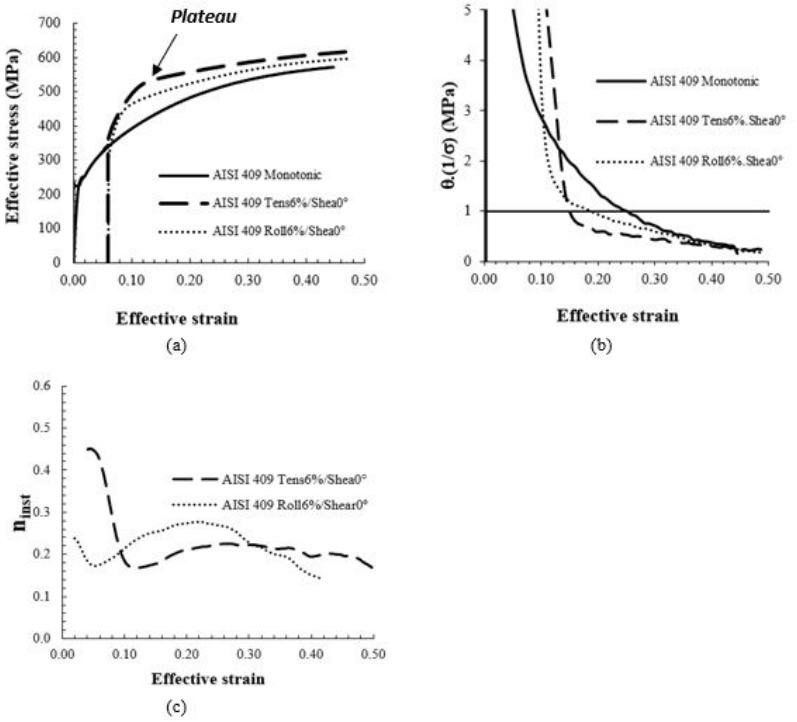

Figure 5. Routes tensile$_{6\%}$/shear$_{0°}$ and rolling$_{6\%}$/shear$_{0°}$: (a) Effective stress-strain curves, (b) normalized work-hardening rate- effective strain and (c) n_{inst} – effective strain, AISI 409.

compared to the monotonic state, being the flow stress nearly 40MPa higher in tensile than in rolling at the beginning of the loading, Figure 5a. Furthermore, the results indicated a greater reduction in the work-hardening for the prestrain in tensile with the increase of the strain in shear, Figure 5b.

A transient hardening stagnation (plateau) was observed in the tensile/shear route, as depicted in Figure 5a. This behaviour is attributed to the movement and arrangement of dislocations, characterized by relatively free movement and the presence of dislocation cell structures during prestrain in tensile, as well as the annihilation of dislocation structures after reloading in shearing. Conversely, the absence of a plateau was correlated with the presence of homogeneous dislocation structures[19].

Both prestrain modes exhibited transient behaviour classified as type 1[20], i.e., higher yield stress which overshoots the monotonic curve followed by a low hardening rate before reassumption as the strain increases in the second deformation mode, shearing, being the opposite for materials that experience yield type 2. The recovery of work-hardening was more pronounced for the rolling/shear route, coherent with the absence of a plateau in this route, as illustrated in Figure 5c by the oscillation of n_{inst} - effective curves, indicating the influence of prestrain mode on the transient plastic behaviour of AISI 409 steel[5,14].

The increase in yield strength observed in both loading routes is typical behaviour of materials subjected to loading sequences with "α" equal to zero. Rauch[21] emphasizes that after a change in the strain path where "α" is zero (orthogonal sequence), new slip systems that were latent in the pre-strain become active. In this manner, the dislocation substructure built in the prestrain of the material (e.g., dislocation walls) acts as an obstacle to dislocation movement during material reloading.

The tensile/shear route exhibited the highest increase in reloading yield stress. Additionally, a higher effective strain value extended the work-hardening rate instability. For the prestrain value of $\varepsilon_{et} = 0.06$, the results suggest that the dislocation substructure developed by the tensile/shear mechanical processing route was more unstable than that observed for the other route, rolling/shear. However, the susceptibility to dynamic recovery phenomena, such as cross slip, can influence the work-hardening of AISI 409 steel after strain path changes[22].

3.3. Effect loading route on the mechanical behaviour of AISI 409

Figure 6 exhibits stress-strain curves for AISI 409 steel for the rolling/tensile/shear route, considering the last effort, shearing, was conducted at 0°and 45° from the previous loading (tensile).

Analogous to the previous routes displayed in Figure 5, the loadings composed of three mechanical efforts also presented higher yield stress and plateau, but differences considering the work-hardening behaviour. For the reloading carried out at 45°, Figure 6b, the effective stress–effective strain curve intersected the respective monotonic loading curve that was not observed at 0°, Figure 6a. The convergence of monotonic and the shear carried out at 45°RD curves was investigated from the analysis of the respective dislocation substructure.

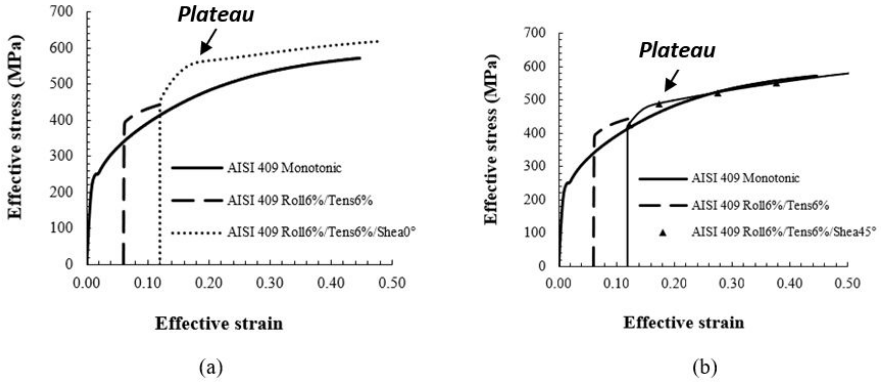

Figure 6. Effective stress-strain curves: routes rolling$_{6\%}$/tensile$_{6\%}$/shear at: (a) 0° and (b) 45°, AISI 409.

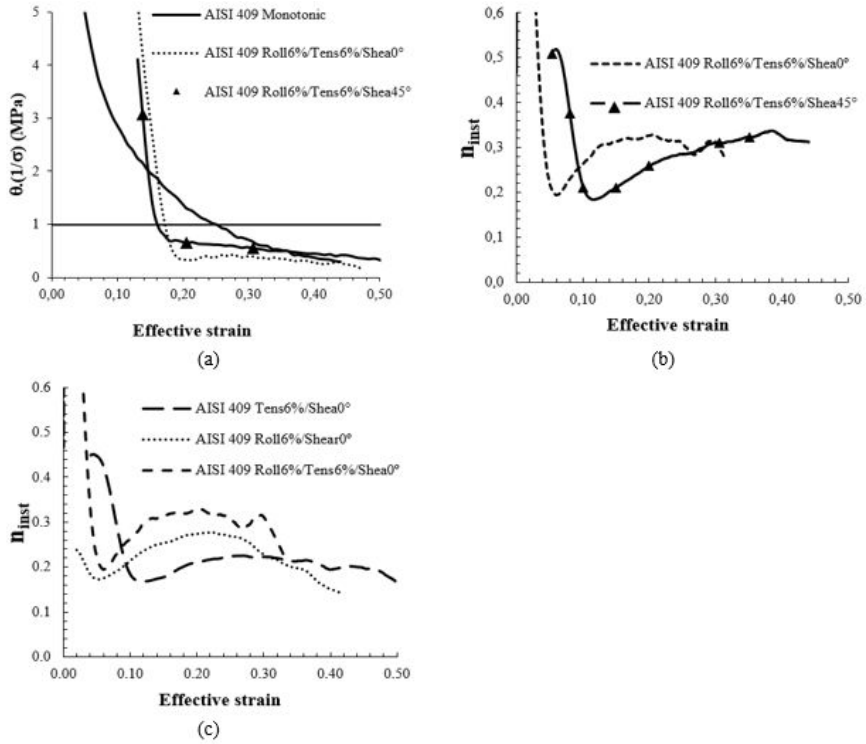

Figure 7. (a) Normalized work-hardening rate-effective strain curves routes tensile$_{6\%}$/shear$_{0°}$ and tensile$_{6\%}$/shear$_{0°}$, (b) n_{inst} – effective strain curves routes rolling$_{6\%}$/ tens$_{6\%}$/shear$_{0°}$ and rolling$_{6\%}$/ tens$_{6\%}$/shear$_{45°}$, (c) n_{inst} – effective strain curves routes tensile$_{6\%}$/shear$_{0°}$, tensile$_{6\%}$/shear$_{0°}$ and rolling$_{6\%}$/ tens$_{6\%}$/shear$_{0°}$, AISI 409.

Concerning the transient in the work-hardening, Figure 7 supports the macroscopic mechanical behaviour depicted in Figures 6a and b. The decrease in the work-hardening rate and the plateau were more intense in rolling/tensile/shear 0º than at 45º, which showed a continuous increment after the initial drop of work-hardening. This result justifies the convergence of stress-strain curves for the shear conducted at 0º.

Figure 7c analyses the effect of prestrain and intermedium modes on work-hardening. It is possible to verify that the minor variation of the work-hardening exponent was detected for the route tens$_{6\%}$/shear$_{0°}$and the higher for the route composed of the three mechanical efforts (route rolling$_{6\%}$/ tens$_{6\%}$/shear$_{0°}$), being associated with the intermedium mode of tensile. It is observed that rolling emphasises the transient concerning the tensile, and the sequence of application of deformation modes affects the intensity of work-hardening fluctuation.

Figures 8 up 10 display the dislocation arrangements for all steps of loading for the rolling/tensile/shear route. In the initial state (as-received) the presence of a low dislocation density is notable when compared to the rolling$_{6\%}$ state, Figures 8a and b, respectively. The loading sequence, rolling$_{6\%}$/tensile$_{6\%}$, revealed establishing a typical columnar dislocation arrangement for the AISI 409 steel, showing

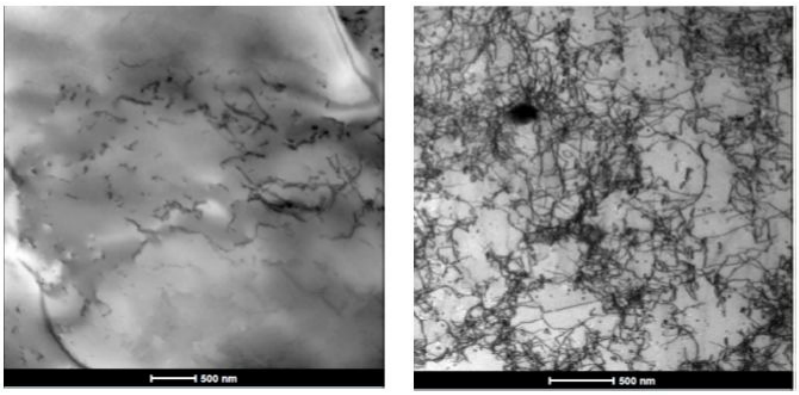

Figure 8. TEM images for the following conditions: (a) as-received and (b) rolling$_{6\%}$, AISI 409.

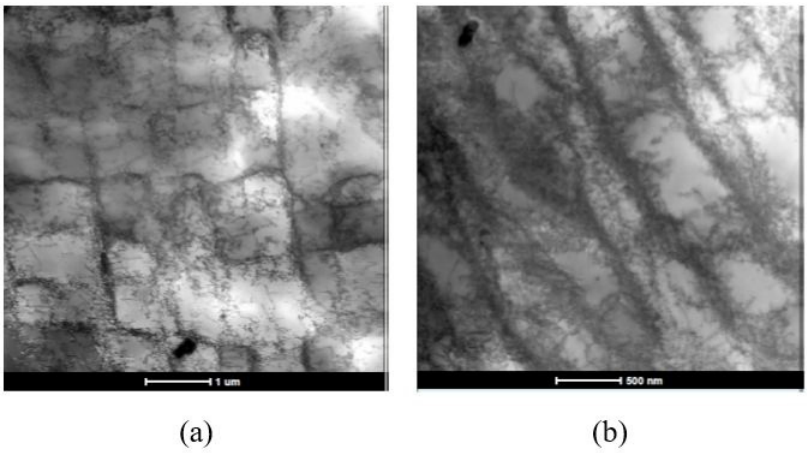

Figure 9. TEM images for the following condition: (a, b) rolling$_{6\%}$/tensile$_{6\%}$, AISI 409.

the effectiveness of the amount of prestrain in rolling and tensile to create a specific dislocation arrangement, Figure 9.

When tensile is used as a prestrain mode on the tensile/shear route, a minor transient in the work-hardening is observed, but when this same effort is an intermedium mode in the rolling/tensile/shear route, this type of loading is responsible for causing the higher oscillation of work-hardening exponent, that modify the dislocation and crystallographic orientation[23,24], among other variables, as the effect of deformation mode on phases transformation that influences the respective mechanical behaviour and the formability of a material[25].

The last step of the loading route, i.e., the shear, indicated slight differences between the respective dislocation substructure created by each angle of the rolling/tensile/shear loading sequence. Figures 10c and 10d exhibit that the dislocation arrangement resulting from shearing conducted at 45° from previous tensile and rolling loading was similar to that observed during the step rolling$_{6\%}$/tensile$_{6\%}$ as shown in Figure 9. This result indicates that the crystallographic orientation established at 45° enhanced the substructure formed during tensile loading. In previous work, in 2022, Morais et al.[26] revealed, from pole figures, a tendency towards reinforced texture on the {1 1 1} and {1 1 0} planes for the route rolling/shear conducted at 45º, indicating a similar configuration occurred for the rolling/tensile/shear route.

This behaviour detected at 45º was opposite that observed at 0°, which was initially modified at the beginning of reloading in shear, as exhibited by the dislocation arrangement for rolling$_{6\%}$/tensile$_{6\%}$/shear$_{0º}$, Figures 10a and b. A partial disruption of dislocation substructure generated during the rolling$_{6\%}$/tensile$_{6\%}$ sequence was observed in this loading sequence, and it can be associated with the occurrence of transient on the work-hardening rate curve displayed in Figure 7a. Although, the increase of plastic deformation in tensile was favourable to the development of another dislocation arrangement typical to the last plastic deformation mode, and consequently, this being correlated with the greater hardening detected in the route rolling$_{6\%}$/tensile$_{6\%}$/shear$_{0º}$[1,27,28].

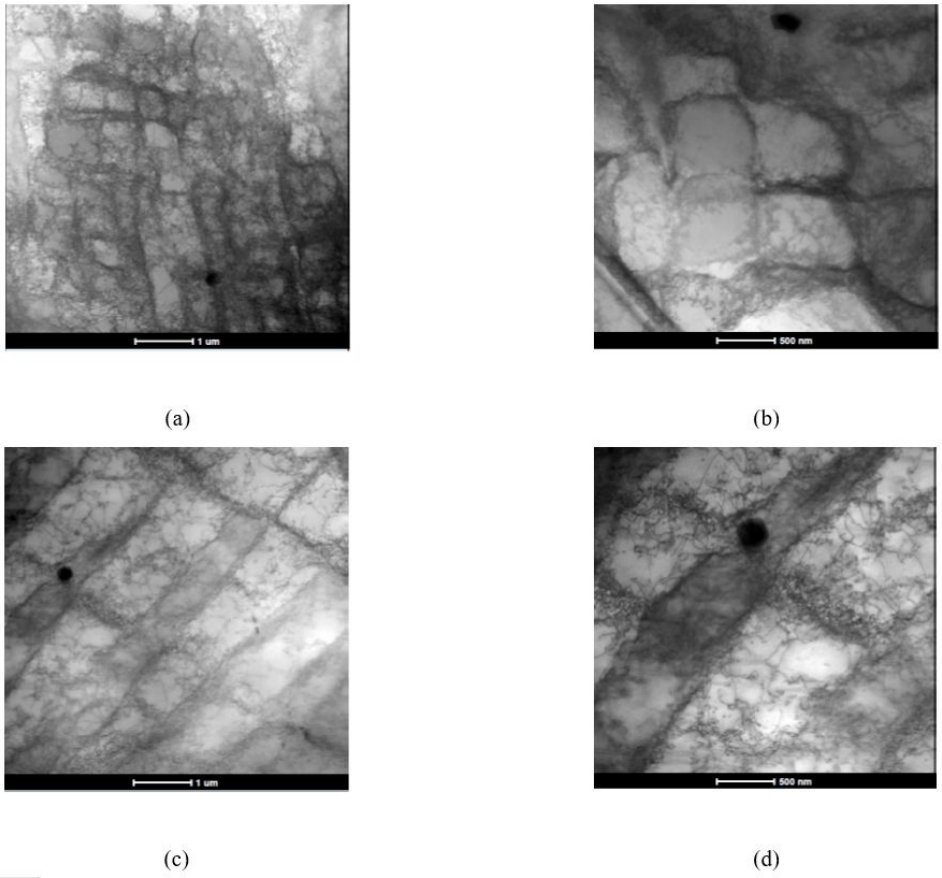

Figure 10. TEM images for the following condition: (a,b) rolling$_{6\%}$/tensile$_{6\%}$/shear$_{0°}$, (c,d) rolling$_{6\%}$/tensile$_{6\%}$/shear$_{45°}$, AISI 409.

The occurrence of transients in the work-hardening rate of AISI 409 steel under the rolling$_{6\%}$/tensile$_{6\%}$/shear$_{0°}$ route should consider the effect of some variables, such as the prior mechanical stresses (cold rolling and tensile), the amount of plastic deformation for each deformation mode, the substructural arrangement and the crystallographic orientation developed during each deformation step[8,26,29,30].

4. Conclusions

This work investigated the effect of strain path changes on the mechanical behaviour and the occurrence of work-hardening transients on the AISI 409 under loading sequences composed of rolling, tensile and shearing efforts. The results indicated the effect of prestrain mode on the occurrence of transient work-hardening rate, with the plateau a marker of dislocation structure disruption.

The mode, sequence and direction of the mechanical efforts applied to the AISI 409 under the rolling/tensile/shear route influenced the development of the dislocation structure and, consequently, the occurrence and intensity of the transient work-hardening rate in addiction to effects associated with texture.

Disruption of dislocation substructure was correlated with the presence and higher intensity of work-hardening rate transient in rolling$_{6\%}$/tensile$_{6\%}$/shear$_{0°}$ route than that observed for rolling$_{6\%}$/tensile$_{6\%}$/shear$_{45°}$.

5. Acknowledgements

The authors are grateful to CEFET-MG (Centro Federal de Educação Tecnológica de Minas Gerais), to CNPq (Conselho Nacional de Desenvolvimento Científico e Tecnológico), to CAPES (Coordenação de Aperfeiçoamento de Pessoal de Nível Superior) and FAPEMIG (Fundação de Amparo à Pesquisa do Estado de Minas Gerais).

6. References

1. Aung TL, Ma N, Okitsu Y, Hayashi S, Takada K, Naito T. Measurement and modelling of strain-path dependent anisotropic hardening behaviors of high strength steels subjected to pre-strains. J Mater Res Technol. 2023;23:451-65.
2. Toroghinejad MR, Taali S, Asgari H, Szpunar JA. The role of strain path changes on the microstructure, texture, and mechanical properties of unidirectionally and cross-accumulative roll-bonded (ARBed) aluminum. J Mater Res Technol. 2023;26:2165-78.
3. Rauch EF. The stresses and work hardening rates of mild steel with different dislocation patterns. Materials Science and Engineering 1997;234-236:653-6.
4. Lee J, Bong HJ, Kim D, Lee MG. Modeling differential permanent softening under strain-path changes in sheet metals using a modified distortional hardening model. Int J Plast. 2020;133:1-10.
5. Aung TL, Ma N, Okitsu Y, Hayashi S, Takada K, Naito T. Measurement and modelling of strain-path dependent anisotropic

hardening behaviors of high strength steels subjected to pre-strains. Int J Mater Res Technol. 2023;23:451-65.
6. Shang M, Yang H, Xing J, Wan J. A unified hardening and damage characterization of Q960 steel under reverse loading. J Construct Steel Res. 2024;217:108659.
7. He W, Meng B, Zheng L, Yang Y, Wan M. Size effect on the cyclic deformation behavior of superalloy ultrathin sheet: characterization and multiscale modelling. Int J Plast. 2023;163:103566.
8. Aung TL, Ma N, Okitsu Y, Hayashi S, Takada K, Naito T. Measurement and modelling of strain-path dependent anisotropic hardening behaviors of high strength steels subjected to pre-strain. J Mater Res Technol. 2023;23:451-65.
9. Schmitt JH, Aernoud E, Baudelet B. Yield loci for polycrystalline metals without texture. Mater Sci Eng. 1985;75:13-20.
10. ASTM: American Society for Testing and Materials. ASTM E112-13: Standard Test Methods for Determining Average Grain Size. West Conshohocken: ASTM International; 2021. https://doi.org/10.1520/E0112-13R21.
11. ASTM: American Society for Testing and Materials. ASTM E8/E8M–24: Standard Test Methods for Tension Testing of Metallic Materials. West Conshohocken: ASTM International; 2024. https://doi.org/doi:10.1520/E0008_E0008M-24.
12. ASTM: American Society for Testing and Materials. ASTM E517–24: Standard Test Method for Plastic Strain Ratio r for sheet metal. West Conshohocken: ASTM International; 2024. https://doi.org/doi:10.1520/E0517-24.
13. Zandrahimi M, Platias S, Price D, Barret D, Bate PS, Roberts WT. Effects of changes in strain path on work hardening in cubic metals. Metall Trans. 1989;20A:2471-82.
14. Gonoring TB, Salustre MGM, Caetano GA, Martins JBR, Orlando MTDA. A constitutive model for the uniaxial tensile plastic behavior of metals based on the instantaneous strain-hardening exponent. J Mater Res Technol. 2022;20:2421-43.
15. Ghafouri M, Afkhami S, Pokka AP, Javaheri V, Togiani A, Larkiola J, et al. Effectof temperature on the plastic flow and strain hardening of direct-quenched ultra-high strength steel S960MC. Thin-walled Struct. 2024;194:111319.
16. Bouvier S, Gardey B, Haddadi H, Teodosiu C. Characterization of the strain-induced plastic anisotropy of rolled sheets by using sequences of simple shear and uniaxial tensile tests. J Mater Process Technol. 2006;174:115-26.
17. Dwivedi PK, Dutta K. Mechanism of ratcheting deformation of HSLA steel: effects of internal stress and dislocation density. Materialia (Oxf). 2023;32:101939.
18. Feng H, Cai L, Wang L, Zhang X, Fang F. Microstructure and strength in ultrastrong cold-drawn carbon steel. J Mater Sci Technol. 2022;97:89-100.
19. Han G, He J, Li S, Lin Z. Simple shear methodology for local structure-property relationships of sheet metals: state-of-art and open issues. Prog Mater Sci. 2024;143:101266.
20. Chung K, Wagoner RH. Effect of stress-strain-law transients on formability. Metall Trans A. 1986;17:1001-9.
21. Rauch EF. The flow law of mild steel under monotonic or complex strain path. Diffus Defect Data Solid State Data Pt B Solid State Phenom. 1992;23-24:317-34.
22. Gao F, Zhu Q, Xue W, Chen Y, Zhang F, Nan Y, et al. Correlation between formability, ridging and recrystallization texture development in ferritic stainless steel fabricated by introducing intermediate annealing during cold rolling. Mater Charact. 2023;205:113296.
23. Inoue T, Ueji R. Effect of strain and deformation mode on cube texture formation in warm bi-axial rolled low-carbon steel. Finite Elem Anal Des. 2021;18:103491.
24. Liu X, Li H, Hu M, Zhu B, Xie C, Zhang X, et al. Effect of deformation mode on double-peak texture evolution in pre-twining Mg-3Al-1Zn alloy during high-speed impacting loading. J Alloys Compd. 2023;968:172122.
25. Satyampet P, Bhunia S, Kundu S, Pant P. Effect of deformation mode on martensitic transformation in medium Mn steel. Materialia (Oxf). 2024;34:102065.
26. Morais FLD, Corrêa ECS, Lopes W. Effect of shear direction on work-hardening evolution of AISI 409 steel under rolling/shearing loading. Mater Res. 2022;25:e20210398.
27. Tekumalla S, Seita M, Zaefferer S. Delineating dislocation structures and residual stresses in additively manufactured alloys. Acta Mater. 2024;262:119413.
28. Kubena I, Fintová S, Jambor M, Smíd M. TKD/EBSD and TEM analysis of microstructural changes ongoing in AISI 304L steel exposed to the cyclic loading. Mater Sci Eng. 2023;872A:144943.
29. Yang Q, Zhang W, Guo Y, Liang F, Yin P, Chang L, et al. A universal constitutive model considering strain range dependence effect and transient behaviour for both cyclic softening and hardening steels. Eng Fract Mech. 2023;290:109481.
30. Wei X, Liu Y, Zhang X. Effect of non-linear tension-compression loading reversal on the hardening behavior and initiation fracture strain of a cold-rolled TRIP780 steel sheet. Mater Today Commun. 2022;30:103076.